Macromolecules
ARTICLE

Macromolecules **2009**, *42*, 8271–8285 **8271**
DOI: 10.1021/ma9016407

Quasielastic Neutron Scattering and Molecular Dynamics Simulation Study on the Structure Factor of Poly(ethylene-*alt*-propylene)

R. Pérez-Aparicio,*,† A. Arbe,‡ F. Alvarez,†,‡ J. Colmenero,†,‡,§ and L. Willner⊥

†*Departamento de Física de Materiales UPV/EHU, Apartado 1072, 20080 San Sebastián, Spain,* ‡*Centro de Física de Materiales (CSIC−UPV/EHU)−Materials Physics Center (MPC), Apartado 1072, 20080 San Sebastián, Spain,* §*Donostia International Physics Center, Paseo Manuel de Lardizabal 4, 20018 San Sebastián, Spain, and* ⊥*Institut für Festkörperforschung, Forschungszentrum Jülich GmbH, D-52425 Jülich, Germany*

Received July 24, 2009; Revised Manuscript Received September 18, 2009

ABSTRACT: By combining neutron scattering and fully atomistic molecular dynamics simulations, we have investigated the static [$S(Q)$] and dynamic [$S(Q,t)$] structure factor of poly(ethylene-*alt*-propylene) in a wide momentum-transfer Q range ($0.2 < Q < 3$ Å^{-1}) spanning over inter- and intramolecular length scales and including also the region of intermediate length scales. The experiments consist of diffraction with polarization analysis and neutron spin-echo measurements on a fully deuterated sample. These results have been used to thoroughly validate the simulations, which have been subsequently exploited to unravel the different contributions to $S(Q)$ and $S(Q,t)$ and provide insights into real space. We have first disentangled the short-range order in this polymer. At the first peak of $S(Q)$ which is clearly dominated by the interchain contribution of the main-chain/main-chain correlations, the dynamics above the glass transition reveal the genuine α-relaxation. The direct observation of the α-relaxation in this way has allowed establishing the viscosity scaling, the stretching, and the deGennes narrowing. An in-phase modulation with $S(Q)$ is observed for the amplitude and shape parameter of the slow decay of $S(Q,t)$ around the first peak. The corresponding time scale also displays a maximum that shifts with temperature in a much stronger way than that of $S(Q)$. Coherency effects in the slow decay are lost above ≈1.5 Å^{-1}, where intramolecular correlations dominate. Interestingly, the apparent activation energy of the characteristic time mirrors the structure factor in the whole Q range investigated.

Introduction

An enormous effort has been made in the past decades to solve the problem of the glass transition. The formulation of theoretical frameworks, in particular the mode coupling theory (MCT),[1−3] has been of utmost importance in this direction. In the late 1980s and during the 1990s, MCT predictions on the behavior of the structural α-relaxation inspired a series of neutron scattering experiments aimed to investigate the dynamic structure factor $S(Q,t)$ (Q: wavenumber) of different glass-formers including, e.g., molten mixed salts,[4] low-molecular-weight systems like *o*-terphenyl[5−7] or glycerol,[8,9] and polymers like 1,4-polybutadiene (PB).[10] The focus was mainly on the direct observation of the decay of the intermolecular correlations, governed by the structural relaxation, in order to check the universal properties predicted for this process, e.g., viscosity scaling and stretching. Therefore, experiments were performed in the vicinity of the first structure factor peak which in amorphous systems usually reflects correlations between the structural units. The Q dependence of the amplitudes of the α- and β-relaxations was also investigated in some cases, like in refs 6, 7, and 10. Despite the big effort invested, unfortunately several questions still remain open.[3]

From an experimental point of view, it is clear that the microscopic information provided by the dynamic structure factor is essential to contribute to the understanding of the dynamics of glass-forming systems, in particular of polymers. During the past years $S(Q,t)$ has been investigated in quite a large number of polymers including polyethylene (PE),[11−13] PB,[10,14,15] polyisoprene (PI),[16] polyisobutylene (PIB),[17,18] atactic polypropylene (a-PP),[19] polyurethane (PU),[20] poly(vinyl chloride) (PVC),[21] poly(vinylethylene) (PVE),[22,23] poly(methyl methacrylate) (PMMA),[24] poly(vinyl acetate) (PVAc),[25] and poly(ethylene oxide) (PEO).[26] Most of these works are based on neutron spin-echo (NSE) measurements[22] in the neighborhood of the first structure factor peak. Extending the Q range toward the second structure factor peak has led to finding clear influences of dynamical processes of intrachain nature, for example in the case of PB.[14,15] In such region, the dynamical peculiarities of each polymer associated with its particular microstructure emerge.

Functions like the structure factor containing collective information on atomic pairs are usually extremely difficult to interpret. Therefore, some recent works have combined neutron scattering results with molecular dynamics (MD) simulations. For the static case, this approach has proven to be highly successful to decipher the short-range order and its relation to the particular microstructure in several glass-forming polymers (see e.g. refs 27−33). Less numerous are the combined studies on collective dynamics.[24−26,34−36] Interestingly enough, the recent works on PMMA and PVAc[24,25] have evidenced the complicated interplay of the correlations contributing to the first structure factor peak. Thus, the observation of the total dynamic structure factor in this Q range does not guarantee the proper characterization of the features of the structural relaxation in those polymers.

Thus, clear difficulties to check theoretical predictions arise from the intrinsic complexity of *real* glass-formers. They partially relate to the delicate identification of the correlations leading to

*To whom correspondence should be addressed. E-mail: r.perezaparicio@ehu.es

Published on Web 10/02/2009

the structure factor peaks. In addition, the relatively complicated microstructure even of systems considered as "model", like e.g. PB, usually leads to rich dynamical behavior associated with internal degrees of freedom in the structural units that may hamper the observation of the universal features seeked by theoretical approaches.[37,38] Therefore, studies on systems as simple as possible might be crucial in this direction. Unfortunately, the simplest polymers, PE and PEO, show a strong tendency to crystallize and therefore are not ideal systems to follow the freezing of the structural relaxation leading to the glassy state. Alternating poly(ethylene-*alt*-propylene) copolymer (PEP), only differing from PE by one methyl group linked to every fourth backbone carbon, provides probably the best compromise: crystallinity is avoided introducing a minimal chemical complexity.

With these ideas in mind, we have performed neutron scattering experiments on a fully deuterated PEP (dPEP) sample: diffraction with polarization analysis has provided the static structure structure factor $S(Q)$ in the glassy state as well as in the supercooled liquid, while the dynamic structure factor has been investigated by means of NSE at temperatures above the glass-transition temperature T_g. With the NSE experiments we have covered Q values from 0.2 to 1.8 $Å^{-1}$. This range includes the region of intermediate length scales and the first structure factor peak, up to the minimum between the first and second peaks. Intermediate length scales correspond to lengths larger than the interparticle distances but smaller than the hydrodynamic regime. The dynamic structure factor at intermediate length scales has been almost unexplored until now. A theoretical framework to predict the $S(Q,t)$ behavior of polymers there is missing, and, to our knowledge, only results on PIB have been reported so far.[17] Therefore, additional information characterizing the behavior of $S(Q,t)$ in this region is extremely interesting in the field of polymer physics. In this work we present a phenomenological description of the experimental data in the whole Q and T range explored.

In order to properly interpret our experimental results, we have combined them with fully atomistic MD simulations. A phenomenological analysis of the simulated data is performed in a parallel way to that followed with the experimental functions. After ensuring the reliability of the simulated cell by comparison with the neutron scattering data, we have exploited the capabilities of the simulation. By using a suitable grouping of the partial correlation functions based on specific molecular groups in the repeat unit—main-chain and methyl group atoms—we have unveiled the origin of the correlations contributing to the diffraction pattern. The radial distribution functions have been studied in real space, separating their inter- and intramolecular contributions. The dynamic structure factor has also been analyzed in terms of the contributions from the main molecular groups. Their comparison with the respective self-terms has allowed determining the coherency effects associated with each kind of correlation. We have checked the validity of the deGennes narrowing prediction with these functions as well as with the experimental results, considering previously reported data on PEP hydrogen self-motions.[39]

Molecular Dynamics Simulations

The fully atomistic molecular dynamics simulations were carried out by using Materials Studio and the DISCOVER module from Accelrys with the COMPASS Force Field (Condensed-phase Optimized Molecular Potentials for Atomistic Simulation Studies). COMPASS is the first ab initio force field that has been parametrized and validated using condensed-phase properties in addition to various ab initio and empirical data for molecules in isolation. Therefore, this force field enables accurate and simultaneous prediction of structural, conformational, vibrational, and thermophysical properties, which exist for a broad range of molecules both isolated and in condensed phases and under a wide range of conditions of temperature and pressure.[40−46] The model cubic cell was built by means of the Amorphous Cell Protocol, originally proposed by Theodorou and Suter,[47] containing polymer chains at a density corresponding to the experimental value for the polymer and with three-dimensional periodic boundary conditions.

Table 1. Details of the Simulated Cells

T (K)	ρ_{exp} (g/cm^3)	ρ_{MDS} (g/cm^3)	cell dimension (Å)
413	0.790	0.7948	52.014
350		0.8266	51.338
300	0.856	0.8549	50.766

In this work, we constructed a cubic cell containing 12 atactic polymer chains of 80 monomer units of PEP, being in total 14 424 atoms, at 300, 350, and 413 K. We started from 12 different well-equilibrated chains, and we constructed a cubic cell with periodic boundary conditions at 413 K and an initial density set to 0.79 g/cm^3, which is the experimental value at that temperature[48,49] (see Table 1). Standard minimization procedures (Polak−Ribière conjugate gradients method) were applied to the constructed cell in order to minimize the so-obtained energy structure. Furthermore, a simulation of 1 ns was run to equilibrate the amorphous cell at 413 K. The equilibrium density of the cell was achieved by running *NPT* dynamics (constant number of atoms, pressure, and temperature in the cell) at fixed atmospheric pressure (P = 0.0001 GPa). After three runs of 1 ns we reached a density of 0.7948 g/cm^3 (close to the experimental value and to the average over the runs), which leads to a cell dimension of 52.014 Å side. Further simulations were carried out in the *NVT* ensemble (constant number of atoms, volume, and temperature) at 413 K. As an integration method, we have used the velocity-Verlet algorithm with a time step of 1 fs. For temperature control instead of a real temperature-bath coupling (i.e., Nosé-Hoover or Berendsen thermostats) we have followed a velocity scaling procedure but with a wide temperature window of 10 K, where greater temperature fluctuations are allowed but the trajectory is disturbed less. In fact, we have checked that by following this simple procedure we obtain results similar to those obtained with a *NVE* ensemble in a similar polymeric system (constant total energy instead of temperature), which has the proper Newtonian dynamics. Thereafter, a simulation of 1 ns was run to equilibrate the sample. Afterward, a simulation of 1 ns was run in this system, collecting data every 0.01 ps. Then, two successive runs of 2 and 100 ns were carried out, collecting data every 0.05 and 0.5 ps, respectively. Finally, an extra run of 1 ns was executed in order to check for the possible appearance of the aging process, but nearly indistinguishable results were obtained from the consecutive simulation runs, confirming local equilibration of the sample.

The so-obtained system was used to generate corresponding cells at the other temperatures, 350 and 300 K. In order to do this, *NPT* simulation runs of some nanoseconds (depending on the temperature) were used to readapt the system to each new temperature, allowing the size of the system to rearrange itself so it could accommodate to the new density at each temperature. In this way, we got the values displayed in Table 1 for the cell sizes and densities. Subsequent *NVT* runs of 1 ns were performed for equilibration at each temperature before collecting data for analysis, in the same way as described above for 413 K.

Correlation Functions and Neutron Scattering Observables

From the atomic trajectories recorded at different times it is possible to calculate different atomic correlations in the sample

cell. For example, the pair correlation functions $g_{\alpha\beta}(r,t)$ can be obtained as

$$g_{\alpha\beta}(r,t) = \frac{1}{N}\langle \sum_{i\alpha,j\beta}^{N_\alpha N_\beta} \delta(r - |\vec{r}_{i\alpha}(t) - \vec{r}_{j\beta}(0)|)\rangle \quad (1)$$

Here the subscripts α and β refer to specific kinds of atoms (e.g., main-chain carbons, methyl group hydrogens, etc.). In eq 1, $\vec{r}_{i\alpha}$ is the position vector of the ith atom of kind α at time t, and N_α, N_β are the total number of atoms of kind α and β in the sample cell. The sum runs over all the different atoms of kind α and β. The average is performed over a large number of frames to get the proper averages. The static case $t = 0$ corresponds to the radial pair probability distribution function.

The results will be partially discussed in the reciprocal space through the structure factors. The Fourier transform of $g_{\alpha\beta}(r,t)$ yields the pair correlation functions $a_{\alpha\beta}(Q,t)$ in Q-space, i.e.

$$a_{\alpha\beta}(Q,t) = \int_0^\infty 4\pi r^2 g_{\alpha\beta}(r,t)\frac{\sin(Qr)}{Qr}\,\mathrm{d}r \quad (2)$$

assuming an isotropic system. The coherently scattered neutron intensity is obtained by adding up all the contributing correlations properly weighted with the scattering lengths of the involved isotopes $\bar{b}_\alpha$ and $\bar{b}_\beta$:

$$I_{\mathrm{coh}}(Q,t) = \sum_{\alpha,\beta}\bar{b}_\alpha\bar{b}_\beta a_{\alpha\beta}(Q,t) = \sum_{\alpha,\beta} A_{\alpha\beta}(Q,t) \quad (3)$$

Here we have introduced the correlation functions $A_{\alpha\beta}(Q,t)$, where each atomic pair correlation has been weighted with its corresponding scattering lengths. The values of the coherent scattering lengths of the isotopes composing the deuterated PEP (dPEP) sample are $\bar{b}_C = 6.6511$ fm and $\bar{b}_D = 6.671$ fm. Because of their almost identical values, the coherently scattered intensity is very close to the true dynamic structure factor $S(Q,t)$ (all atoms equally weighted). In a diffraction experiment addressing differential cross sections, this corresponds to the true static structure factor $S(Q)$. For this reason, we will extend the use of the terms $S(Q,t)$ [$S(Q)$] to denote the function expressed by eq 3 (eq 3 for $t = 0$) when a fully deuterated sample is considered. The self-part of the dynamic structure factor is the result of eq 3 when restricting the sum in eq 1 to the terms $i\alpha = j\beta$, normalized to its static value. In an analogous way the self-counterparts of the correlation functions $A_{\alpha\beta}(Q,t)$ can be calculated.

The coherent cross section per monomer is determined as $\sigma_{\mathrm{coh}} = \sum\bar{b}_\alpha\bar{b}_\beta$, where the sum extends over all the atoms of the monomer. For deuterated PEP (see chemical composition in the inset of Figure 1a), $\sigma_{\mathrm{coh}}^{\mathrm{dPEP}} = 83.715$ barns/monomer (1 barn = 100 fm^2). We note that the total neutron intensity scattered also contains an incoherent contribution. The incoherent cross section per monomer is obtained as $\sigma_{\mathrm{inc}} = \sum\sigma_{\mathrm{inc}}^{\alpha}$, considering again all the atoms of the monomer. As $\sigma_{\mathrm{inc}}^{\mathrm{C}} = 0$, in a perfectly deuterated sample incoherent scattering arises from deuterons ($\sigma_{\mathrm{inc}}^{\mathrm{D}} = 2.05$ barns) and is rather weak ($\sigma_{\mathrm{inc}}^{\mathrm{dPEP}} = 20.5$ barns/monomer). However, because of the large value of the incoherent cross section of hydrogen ($\sigma_{\mathrm{inc}}^{\mathrm{H}} = 80.27$ barns), we note that the incoherent contribution can be overwhelming in samples with a relatively small amount of hydrogens.

Experimental Section

Sample. Alternating poly(ethylene-*alt*-propylene) copolymer was prepared via saturation of the precursor polydiene polyisoprene. Polyisoprene was obtained via standard anionic polymerization techniques[50,51] using *sec*-butyllithium as initiator and benzene as polymerization solvent. Isoprene-d_8 was purchased from Cambridge Isotope Laboratories, Andover, MA. The degree of deuteration was specified to be 98%. The saturation with deuterium was done with a conventional palladium on barium sulfate catalyst. The polydispersity of the polymer, M_w/M_n, was smaller than 1.05 as determined by size exclusion chromatography (SEC). An absolute molecular weight M_w = 200 kg/mol was obtained by SEC combined with a triple detector array from Viscotek, Model 300. A value of 213 K for the glass transition temperature was determined by DSC.

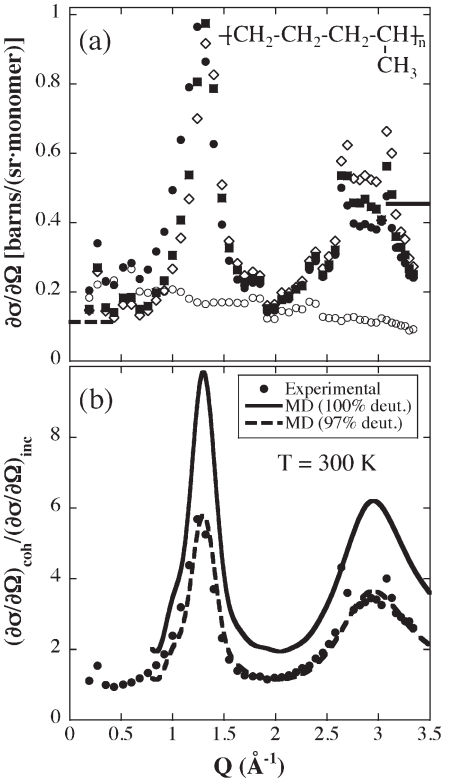

Figure 1. (a) Coherent differential cross sections of dPEP measured by DNS at 10 K (empty diamonds), 200 K(squares), and 300 K (circles). The incoherent differential cross section measured at 300 K (empty circles) is also shown. The horizontal lines show the expected values for the incoherent (left) and coherent (right) theoretical contributions. The chemical formula of PEP is also shown. (b) Ratio of coherent to incoherent differential cross sections from DNS experiments at 300 K (circles) and calculated from the MD simulations at the same temperature, assuming 100% (solid line) and 97% deuteration level (dashed line).

Neutron Scattering. *Structure: Neutron Diffraction with Polarization Analysis.* DNS (FRJ2-reactor, Forschungszentrum Jülich, Germany) and D7[52] (Institut Laue−Langevin, ILL, Grenoble, France) are diffuse scattering spectrometers capable of three directional polarization analysis. The instruments were used in diffraction mode. In this way an integration over all possible energy values is performed, to finally obtain differential scattering cross sections. In an ideal situation, the incoherent contribution to the differential cross section is equal to $\sigma_{\mathrm{inc}}/4\pi$—and thus independent of Q—and the coherent part reveals the structure factor. The two contributions can be separated by the use of polarized neutrons, since the incoherent scattering arising solely from spin disorder makes the neutron spin flip with a probability of 2/3, while coherent scattering leaves the spin unchanged. At DNS the incident neutron wavelength λ was set to 3.3 Å to cover a Q range from 0.19 to 3.34 Å^{-1}, while at D7 with $\lambda = 4.8$ Å we explored from 0.23 to 2.5 Å^{-1}. The samples were prepared to present a perpendicular neutron transmission of 90%. At DNS, the sample (thickness 0.5 mm) was placed in a hollow cylinder, while a flat niobium container was used at D7. There, the 1 mm thickness sample was placed at 135° with respect to the incident beam. dPEP was investigated at 10, 200,

and 300 K by means of DNS and at 300 and 400 K by D7. Measuring times of about 1.5 h were employed. The correction for background scattering was done by measuring the intensity scattered by the empty cell. A vanadium sheet of 0.5 mm thickness was used to calibrate the detector efficiency and obtain cross sections in absolute units.

Dynamics: Neutron Spin Echo. IN11: The dynamical measurements were carried out using the neutron spin-echo (NSE) technique which offers the highest energy resolution in neutron scattering. In addition, NSE is a unique technique since it determines the intermediate scattering functions directly in the time domain. This is achieved by coding the energy transfer in the scattering process for each neutron individually into its spin rotation.[53] In this way, the application of precession magnetic fields before and after the scattering event results in a polarization of the neutron that depends only on the velocity difference of each neutron individually, irrespective of its initial velocity. Energy resolution and monochromization of the incident beam are decoupled, and resolutions in energy of the order of $\Delta E/E \approx 10^{-5}$ can be achieved with an incident neutron spectrum of 20% bandwidth. These experiments finally access the normalized function

$$\mathrm{NSE}(Q,t) = \frac{I_{\mathrm{coh}}(Q,t) - \frac{1}{3} I_{\mathrm{inc}}(Q,t)}{I_{\mathrm{coh}}(Q,0) - \frac{1}{3} I_{\mathrm{inc}}(Q,0)} \qquad (4)$$

which for fully deuterated samples, to a good approximation, can be identified with the normalized dynamic structure factor $S(Q,t)/S(Q)$. The NSE measurements on the dPEP sample previously investigated at D7 were made at the IN11 instrument also at the ILL. A neutron wavelength of 5.5 Å was used, covering Fourier times between 5.3 and 951 ps. We used the IN11c option, where a multidetector simultaneously covers an angular range of 30° in the horizontal plane. Placing the multidetector at three different angles with respect to the incident beam we gained access to Q values ranging from 0.25 to 1.71 Å^{-1}. Measurements were performed at three temperatures well above the glass transition, namely 300, 350, and 400 K. Measuring time for each detector position and temperature was about 4 h. The instrumental resolution was measured for the same time on the sample at 10 K. As NSE works in the time domain, the deconvolution of the measured spectra from resolution can be realized by simple division of the data collected at the temperature of interest by the instrumental resolution spectrum. The weak background signal was carefully measured and subtracted from the experimental data using the appropriate transmission factors.

Results, Data Analysis, and Validation

Static Structure Factor. Figure 1a shows the DNS results obtained on the coherent dPEP signal at the three temperatures investigated. The revealed structure factor is characterized by a first strong peak at around $Q_{1\max} = 1.25-1.3$ Å^{-1} and a broad second peak in the Q regime $2.2 \le Q \le 3.5$ Å^{-1}. The scatter of data points in the region around 2.7 Å^{-1} is due to the Debye−Scherrer rings of the sample container, which could not be fully subtracted. Above T_g, the first peak is observed to broaden in its low-Q flank and shift its maximum position toward lower Q values, suggesting an interchain origin.[54] In the Bragg approximation, its position reveals an average interchain distance of about $d_{\mathrm{chain}} \approx 2\pi/Q_{1\max} \approx 5$ Å. The second peak is little affected by temperature and must relate to a large extent to intrachain correlations governed by covalent bonds. Very similar behavior is shown by other linear homopolymers; PE displays an almost identical structure factor;[11,12,55,56] a slightly more compact packing would be inferred for PEO[57] and PB,[31,54,58] for which $d_{\mathrm{chain}} \approx 4.3$ Å; on the contrary, PVC's first peak is located at a somewhat smaller Q value corresponding to $d_{\mathrm{chain}} \approx 5.3$ Å. Also, PIB with two methyl groups in the monomer shows a qualitatively identical two-peak structure factor, which reveals a larger associated intermolecular distance (≈6.3 Å).[17] Polymers with more complex microstructure containing bulky side groups usually show more than one peak in the region 0.5−2 Å^{-1} (e.g., PVE,[23] PMMA,[32] PVAc,[25] or polystyrene (PS)[33,59,60]).

In the same Figure 1a, the featureless incoherent contribution measured at 300 K as well as the theoretical incoherent ($\sigma_{\mathrm{inc}}/4\pi$) and coherent ($\sigma_{\mathrm{coh}}/4\pi$) levels are shown for comparison. While the coherent differential cross section should assume the theoretically calculated value only asymptotically in the high-Q limit, the incoherent contribution should be ideally Q-independent and equal to the theoretical expectation. The weak decay of the incoherent differential cross section with increasing Q can be attributed to inelasticity effects.[61,62] On the other hand, a remaining fraction of hydrogens in the sample would be the reason for measuring values higher than the theoretically predicted. In Figure 1b, we have plotted the ratio of coherent to incoherent intensities from the experiment. In this way one cancels out the normalization parameters used to calculate the absolute intensities and avoids uncertainties related to the determination of the absolute cross sections from the experiments. In this figure, the same function but obtained from our MD simulations is displayed for comparison.[63] Assuming perfect 100% deuteration, the calculated ratio of the two intensities is higher than the experimental one. This points out again the presence of protons in the dPEP sample. A little fraction of protons would not appreciably change the coherent signal but visibly increase the incoherent level. By assuming that the Q dependence of the coherent scattering remains the same, we have varied the ratio between coherent and incoherent intensities. The value which best matches simulated and experimental data (see Figure 1b) corresponds to a proton content of 3%. This value is compatible with the nominal deuteration level of this sample. Assuming this degree of deuteration in the real sample, we observe a perfect agreement between experimental and simulation results at room temperature. As we will see later, the temperature dependence of the structure factor is also well mimicked by the simulations. This comparison allows us to validate the simulated cell—at least regarding the short-range order aspects.

Dynamic Structure Factor. In Figure 2 we can see the dynamic structure factor normalized to its static value as calculated from the MD simulations at the three temperatures investigated and for different Q values around its first peak. In all cases the structure factor relaxes in two steps. In a first fast regime below 1−2 ps—governed by the so-called "fast dynamics" or "fast process"—the correlations decay down to a level that depends on both Q and temperature. The complete decay of the function is only realized through a second slow mechanism which characteristic time scale is also strongly Q- and T-dependent. In order to compare the MD simulation results with those obtained from NSE, the amplitudes of the latter have to be first corrected for band-pass effects. They consist of a deficient normalization of the NSE signal (determination of the denominator in eq 4). At the used wavelengths the IN11C band-pass allows for energy transfers up to about 2 meV. Thus, the normalization would include the so-called fast processes observed at energies below about 2 meV but excludes the ordinary vibrations. To estimate the difference between the full integral and that performed by the instrument, we have "calibrated" the NSE results by comparing measurements at "$t_{\mathrm{exp}} = 0$" and simulation data at different times on a fully protonated

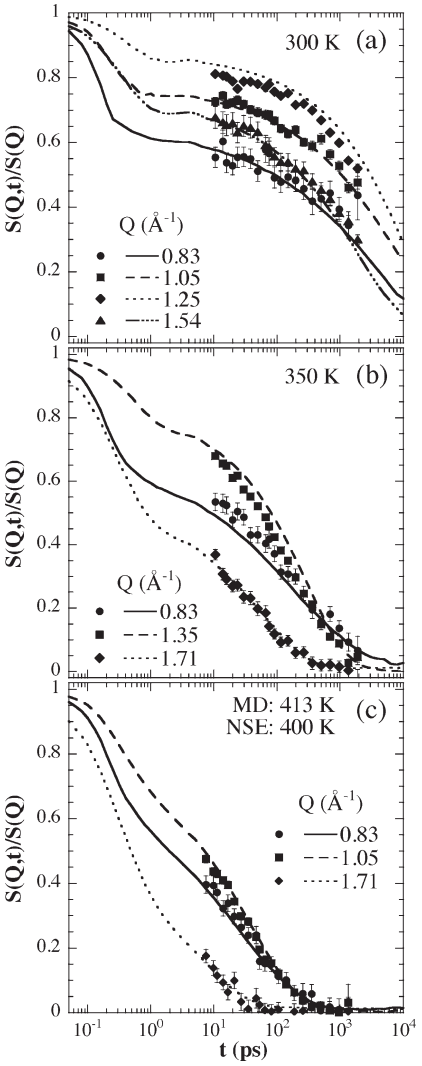

Figure 2. Normalized dynamic structure factor measured by IN11 (symbols) and calculated from the MD simulations (lines) at the different temperatures investigated ((a) 300 K, (b) 350 K, and (c) 400 K for the experiments and 413 K for MD) and the specified Q values. The amplitudes of the experimental data have been corrected for the band-pass of the spectrometer using MD simulations results at $t = 0.16$ ps. Shift in the experimental time scales have also been applied in order to match both sets of results (see text).

PEP sample (incoherent scattering).[64,65] An overall agreement is achieved for a simulated time of 0.16 ps. We have thus assumed that the effect of the band-pass can be well approximated by the decay of the correlation function at this time, which can be determined by computing the corresponding measured function from the simulations. In the case of the deuterated sample, at the maximum of $S(Q)$ these corrections are only of the order of about 5%, while they become more important when moving toward lower or higher Qs, amounting to about 20% in the extremes of the window experimentally explored. Applying these band-pass corrections (that only affect the amplitudes), a constant shift in the time scale is appreciated between the NSE and the MD simulation data—the experimental curves decay at slightly faster times. For each temperature, we have estimated the shift in time scales that better matches NSE and simulated data. This shift is of 0.3 decade for 300 and 350 K, while the experimental curves at 400 K match well the 413 K simulated results if the shift amounts to 0.15 decade. Figure 2 shows the comparison between simulation and experiment assuming

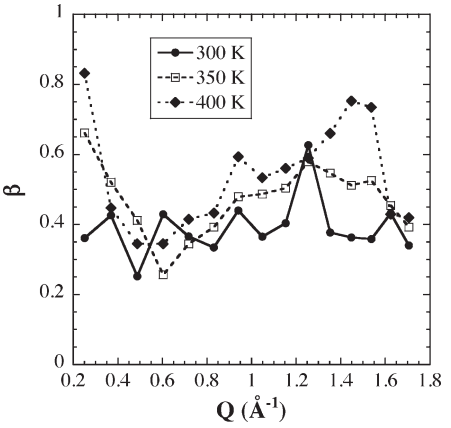

Figure 3. Momentum transfer dependence of the KWW shape parameter characterizing the slow decay of the NSE data at the three temperatures investigated.

such shifts. As can be appreciated, the agreement is excellent. The spectral shape as well as the Q dependence of the dynamic structure factor is perfectly reproduced by the simulations. We note that the shift applied is needed to match the *slow* decay and could reflect a slight mismatching of the intermolecular potentials. We would not expect to have such a shift in the regime of the fast decay, which is more sensitive to intramolecular potentials.[38] Therefore, the band-pass corrections are expected to be still valid—they should be independent of the shift needed for the slow decay. Thus, we can conclude that from a dynamic point of view our cell is properly validated assuming that the slow dynamics in the simulations is slightly slower (a factor 2) than in the real system. As we will see in the following, the analysis of the data will further support this validation.

We first focus on the characterization of the experimental results. The first fast regime below some picoseconds is not accessible by NSE, which is sensitive to the decay in the slow regime. However, the influence of the fast processes is reflected in the amplitude of the experimentally observed decays and can be parametrized by a Debye−Waller factor (DWF). On the other hand, the slow decay shows a stretched form. In glass-forming polymers the normalized dynamic structure factor above some picoseconds can usually be well described by the Kohlrausch−Williams−Watts (KWW) functional form:[22]

$$\frac{S(Q,t)}{S(Q)} = \mathrm{DWF}\exp\left[-\left(\frac{t}{\tau_w}\right)^{\beta}\right] \qquad (5)$$

Here β is the stretching parameter describing the deviations from exponential behavior, and τ_w is the characteristic time which may depend on both Q and temperature. The determination of β from independent fits of eq 5 to the experimental data is subjected to large uncertainties due to the coupling of amplitude and shape parameters. Figure 3 shows the results obtained for the shape parameter from such an analysis of individual spectra. Within the large dispersion of the values, we can deduce a certain tendency of the function to further stretching toward low temperatures: $\langle\beta\rangle(400\ \mathrm{K}) = 0.60$, $\langle\beta\rangle(350\ \mathrm{K}) = 0.50$, $\langle\beta\rangle(300\ \mathrm{K}) = 0.40$. On the other hand, a certain $S(Q)$ modulation of the shape parameter could be envisaged for the two higher temperatures. However, the dispersion of the results is too high, and we have followed the procedure usually reported in the literature for analyzing the experimentally obtained dynamic structure factor.[22] This procedure is based on the construction of

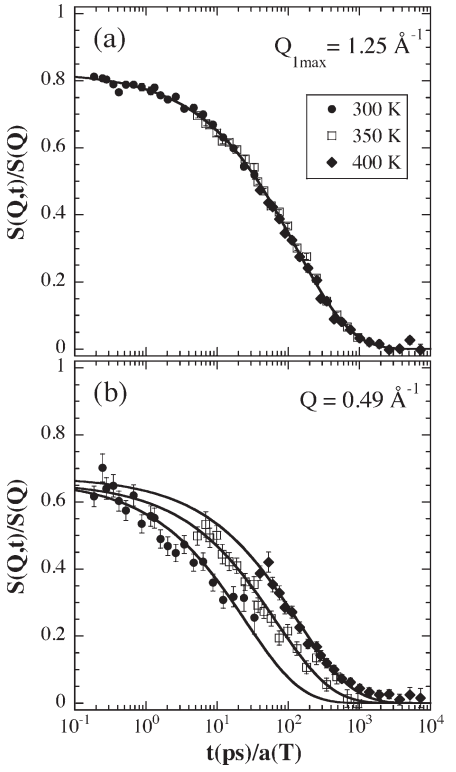

Figure 4. (a) Master curve obtained from the IN11 data at Q = 1.25 Å^{-1} ($\approx Q_{1max}$) applying the viscosity shift factors reported in ref 66. The reference temperature is 350 K. The solid line shows the fit to KWW equation, delivering a β value of 0.56. The same shift factors do not superimpose the dynamic structure factor in the intermediate length scales region, e.g., (b) Q = 0.49 Å^{-1}. Lines in (b) are KWW fits with β = 0.56.

master curves starting from NSE data at different temperatures by scaling the time scales with the temperature dependence deduced from viscosity measurements. Rheological results on PEP[39,66] show that the time scale of the α-process follows a non-Arrhenius-like behavior that is accounted for by the usual Vogel−Fulcher (VF) functional form

$$\tau = \tau_0 \exp\left(\frac{B}{T - T_0}\right) \quad (6)$$

with values B = 2109.2 and T_0 = 145.7 K. Figure 4a shows the results of such a scaling for Q = 1.25 Å^{-1} ($\approx Q_{1max}$). At this Q value, after the phenomenological previous discussion, the structure factor reflects correlations of interchain origin, and thus NSE would reveal the genuine structural relaxation.[1] The excellent scaling observed at Q_{1max} implies that (i) the macroscopically determined temperature dependence of the viscosity follows the microscopically observed decay of the dynamic structure factor at the first amorphous halo; (ii) within the experimental uncertainties the time−temperature superposition principle is well fulfilled; and (iii) the DWF does not depend on temperature, at least in the temperature range investigated. These findings support MCT predictions. We note however that the same shift factors clearly fail superimposing the dynamic structure factor in the intermediate length scales region (Figure 4b). A description of the master curve at Q_{1max} in terms of KWW delivers a β value of β = 0.56 (Figure 4a). Within the uncertainties, the spectral shape of all the experimental data, for all Q and T values, can be well described with this value of β (see, e.g., the fits in Figure 4b). Therefore, to characterize

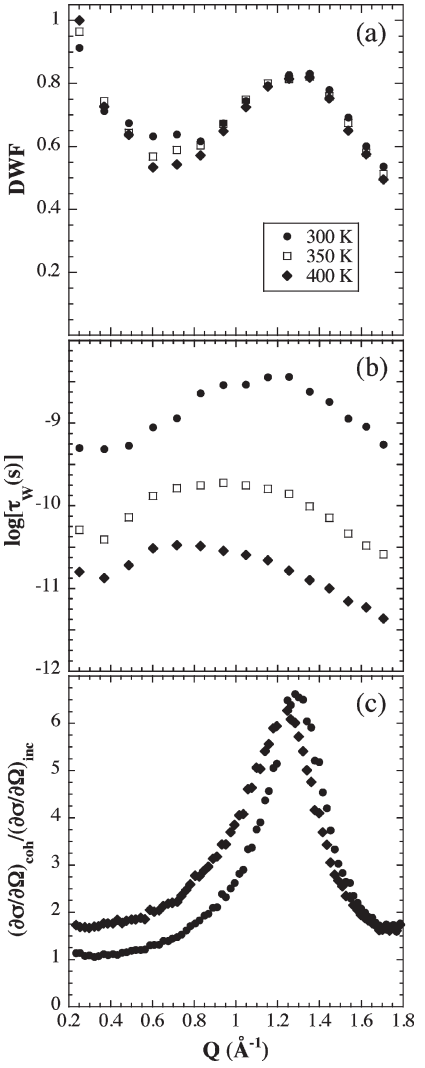

Figure 5. Momentum transfer dependence of the parameters characterizing the slow decay of the experimental dynamic structure factor at the temperatures investigated: (a) DWF and (b) KWW time scales. (c) Static structure factor (ratio of coherent to incoherent differential cross sections) measured by D7.

the decays a common fixed β = 0.56 has been used. The values obtained from such fits for the DWF and the time scales are shown in Figure 5a,b in comparison with the structure factor measured at D7 in the same temperature interval (Figure 5c). Clear modulations related to $S(Q)$ are present in the dynamic parameters. While in the accessed Q range the DWF is practically insensitive to thermal changes, the maximum in the time scales strongly shifts toward lower Q values with increasing temperature. Interestingly enough, this shift is much more marked than that experienced by the first structure factor peak in the same temperature range.

Our results on the time scale imply that its Q and T dependencies cannot be factorized. This is clearly demonstrated in Figure 6a, where the rheological shift factors have been applied to the characteristic time scales of the slow decay obtained from the KWW fits. They are superimposed only in a narrow Q range around 1.3 Å^{-1}. Particularly in the intermediate length scales region, this scaling is definitely not fulfilled. In order to characterize the temperature dependence of the time scales as a function of momentum transfer, we analyzed them in terms of Arrhenius laws for each Q value separately, determining thereby the apparent activation energy $E_a(Q)$. The results are shown in Figure 6b.

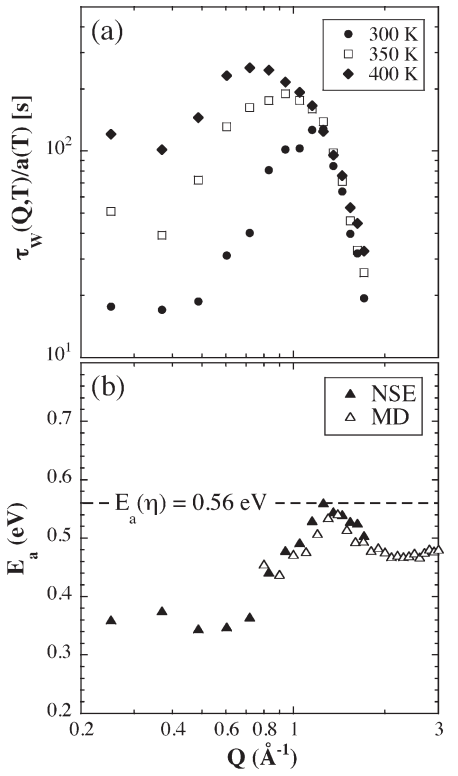

Figure 6. (a) Momentum transfer dependence of the characteristic time of the KWW functions describing the slow decay of the experimental dynamic structure factor at the temperatures investigated. The data have been shifted according to the viscosity shift factors,[66] taking 350 K as the reference temperature. (b) Q dependence of the apparent activation energy obtained from experimental data (full symbols) and from MD simulations (empty symbols). The horizontal line indicates the effective activation energy of the viscosity.

The horizontal line indicates the effective activation energy of the viscosity in the temperature range of observation ($E_a(\eta) = 0.56$ eV). The activation energy of the NSE data follows a kind of modulation with the structure factor, reaching the value of the macroscopic viscosity only in the close vicinity of the structure factor peak. In the intermediate length-scales region, the activation energy seems to approach an asymptotic value of about 0.35 eV.

Now we focus on the simulation results. In this case, the large dynamic window covered makes possible fitting the data with eq 5 without fixing the stretching exponent.[67] The values such obtained for the fitting parameters are shown as symbols in Figure 7a−c. They clearly mirror the Q dependence of $S(Q)$ (see the simulated structure factor in Figure 7d). For comparison, we have also considered the self-part of the dynamic structure factor. This function is an average over the self-motions of all nuclei in the system (deuterons as well as carbons). The analogous fit of eq 5 (with a Lamb−Mössbauer factor (LMF) instead of the DWF) to the self-functions delivers the values of the parameters also included in Figure 7a−c as lines. The self-correlations naturally lack structural reminiscences.

The β-parameter for the self-correlation function (β_{self}) has a tendency to increase with increasing temperature and decreasing Q value. Its coherent counterpart (β_{coh}) clearly marks a maximum at the first $S(Q)$ peak position and stays close but slightly above β_{self} for high Q values, at least for the two lowest temperatures where it can be independently determined. We note that in the overlapping Q range the experimental data suggested an analogous behavior to that observed for β_{coh} from the simulations. In the neighborhood

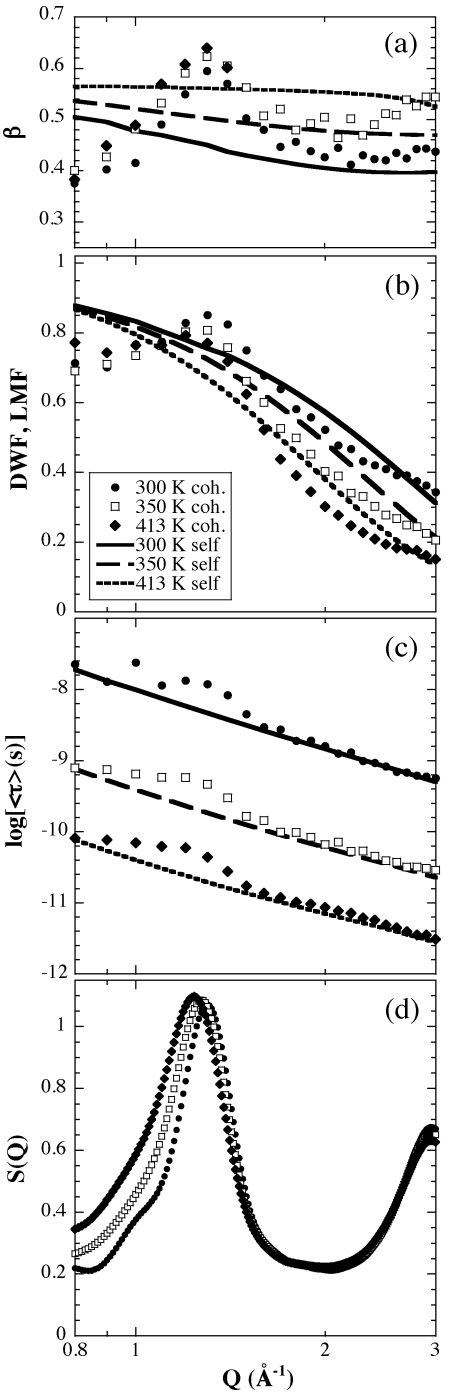

Figure 7. Momentum transfer dependence of the parameters characterizing the slow decay of the simulated dynamic structure factor (symbols) and its self-contribution (lines) at the three temperatures investigated: (a) shape parameters, (b) amplitudes, and (c) average characteristic times. In (d) the simulated static structure factor is shown.

of the maximum, the experimentally determined value ($\beta = 0.56$) can be considered as a good approach to the average value obtained from the simulations. This finding supports the analysis performed and the validation of the simulations.

The DWF of the simulated dynamic structure factor is also modulated by $S(Q)$. This amplitude parameter strongly decreases when the Q range is extended toward Q values larger than those experimentally explored. In this high-Q range, a clear temperature dependence is observed that is absent in the neighborhood of the first structure factor peak. We observe that in fact the coherent amplitudes "surround"

those obtained for the self-correlations (LMF). The later can be well described in terms of the mean-squared displacement $\langle u^2 \rangle$ of the atoms in the fast regime by means of the expression

$$\mathrm{LMF} = \exp\left(-\frac{\langle u^2 \rangle}{3} Q^2\right) \tag{7}$$

Values of 0.39, 0.52, and 0.72 Å^2 are obtained for $\langle u^2 \rangle$ at 300, 350, and 413 K, respectively. They are slightly smaller than those deduced for hydrogen atoms in protonated PEP[39] at the same temperatures (0.42, 0.65, and 0.84 Å^2). As mentioned above, the displacements involved in the self-correlation function here considered are an average over C and D atoms. We expect the mobility in the fast dynamics regime to be spatially more restricted for carbons than for deuterons or hydrogens. Therefore, present results are perfectly compatible with previous experimental data, providing additional support to the reliability of our simulated cell.

Because of the Q, T, and correlator dependence of the shape parameters, we have chosen the average values of the characteristic times $\langle \tau \rangle$ as more adequate to compare the time scales in Figure 7c. For KWW functional forms, they can be obtained from the τ_w and β values through

$$\langle \tau \rangle = \frac{\tau_w}{\beta} \Gamma\left(\frac{1}{\beta}\right) \tag{8}$$

Collective and self-time scales are nearly identical for Q values above $\approx$ 1.5 Å^{-1}. Below, the average times of the dynamic structure factor show a broad peak in a similar way as the experimental time scales do (Figure 5b). We have calculated the Q-dependent apparent activation energies also from the simulated data. The results are directly compared with the experimental ones in Figure 6b. In the overlapping region, the agreement between both sets of data is astonishingly good. The simulation results nicely complement those obtained from NSE toward high Qs. Seemingly, the $Q \rightarrow \infty$ asymptotic value of the apparent activation energy is intermediate between those exhibited by the viscosity and the dynamic structure factor in the intermediate length scales region.

Thus, with this thorough comparison between simulation and experimental results on the dynamic structure factor we have shown that in the overlapping Q region they are—with exception of a factor of 2 in the time scales—nearly identical, validating the cell also from a dynamical point of view. We also conclude from inspection of the structure factors shown in Figure 5c and Figure 7d that the temperature dependence of the structure is also fairly well reproduced.

In the next section we further discuss the results here presented. Taking advantage of the possibilities offered by the extensive information available from the now validated simulations, we can have insight in magnitudes that are not experimentally accessible and that can be of utmost interest to interpret the observations. The first application is to disentangle the structural details giving rise to the short-range order of PEP.

Discussion

Structure: Short-Range Order of PEP. *Contributions to the Static Structure Factor.* The monomer unit of PEP contains 15 atoms. We can identify 8 different species in the monomer unit to extract the different partial correlations. This leads to 36 different partial correlation functions $g_{\alpha\beta}(r)$ or, in Q-space, $a_{\alpha\beta}(Q)$. Analyzing them separately is tedious, and finally it is difficult to visualize the physics behind. Therefore, we have considered some species together to obtain more useful correlations between the relevant molecular groups. We have distinguished two different groups of atoms out of the monomer: the main-chain atoms (MC), which contains the four backbone carbons and the corresponding seven deuterons, and the methyl group (MG) (see inset in Figure 8). With this grouping, we have two partial correlation functions involving correlations among the atoms belonging to the same group, namely MCMC (the contribution arising from main chain) and MGMG (that arising from the methyl group). This grouping also leads to a cross-correlation term relating atoms from one group with atoms from other groups (MCMG). We first focus on the lowest temperature considered, 300 K. With solid lines, Figure 8 shows the three partial correlation functions $A_{\alpha\beta}(Q)$ contributing to the structure factor measured by neutron scattering [$S(Q)$, black line] at this temperature. For obtaining these functions, each atomic pair correlation has been weighted with its corresponding scattering lengths (eq 3). From their inspection, we can extract the following information:

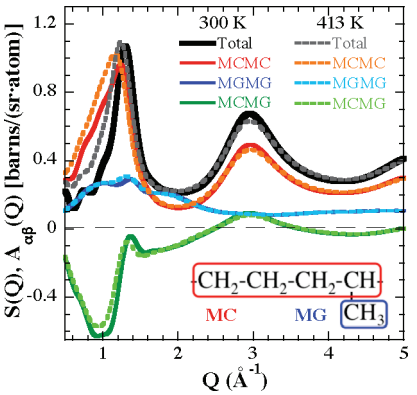

Figure 8. Contributions to the static structure factor calculated from simulations at 300 K (solid lines) and 413 K (dotted lines).

(i) Qualitatively, the total structure factor is very similar to the partial correlation involving MC atoms: below 4 Å^{-1}, both functions display two clear maxima with very similar positions [$Q_{1\mathrm{max}}^{\mathrm{total}}$ = 1.3 Å^{-1}, $Q_{1\mathrm{max}}^{\mathrm{MCMC}}$ = 1.24 Å^{-1}, $Q_{2\mathrm{max}}^{\mathrm{total}} = Q_{2\mathrm{max}}^{\mathrm{MCMC}}$ = 2.95 Å^{-1}] and relative heights.

(ii) The MGMG correlations globally show a very broad feature in the same Q region as the first maximum of the MCMC correlation function. Looking in detail, three distinct contributions centered at $Q_{1\mathrm{max}}^{\mathrm{MGMG}}$ = 0.95 Å^{-1}, $Q_{2\mathrm{max}}^{\mathrm{MGMG}}$ = 1.4 Å^{-1}, and $Q_{3\mathrm{max}}^{\mathrm{MGMG}}$ = 1.9 Å^{-1} could be discriminated in this broad peak. At higher Q values, the function is almost flat.

(iii) Above $Q \approx 2$ Å^{-1}, the cross-term MCMG mirrors the MCMC correlations. Below, the main feature is a marked negative peak centered at $Q \approx 0.95$ Å^{-1}, i.e., where the first peak is observed for the MGMG correlation function ($Q_{1\mathrm{max}}^{\mathrm{MGMG}}$). It is the strong negative contribution of the MCMG term in this Q range which leads to a sharper first peak for $S(Q)$ than that displayed by the MCMC correlations only—the main difference between both functions. Finally, we note a similar feature (maximum) of MCMG and MGMG correlations at Q = 1.4 Å^{-1} [$Q_{2\mathrm{max}}^{\mathrm{MGMG}}$].

In the same Figure 8 we can appreciate the temperature dependence of these correlations, since the dotted lines

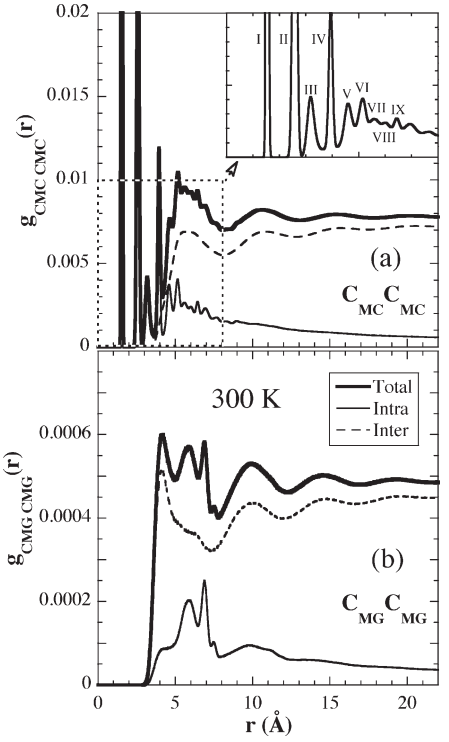

Figure 9. Radial pair correlation function at 300 K, relating (a) carbons in the main chain (CMC) and (b) carbons in the methyl group (CMG), calculated from the MD simulations. The dashed lines show the interchain correlations, the solid lines the intrachain correlations, and the thick solid lines the total functions. The inset in (a) is a zoom of the selected area showing the assignation of the different intrachain peaks.

display the results at 413 K. As in the case of the experimental results, the main thermal effects are found at Q values below $Q \approx 1.5$ Å^{-1}. There, while the first peak of A_{MCMC} and the second peak of A_{MGMG} show an influence of temperature, this is absent in the first and third peaks of A_{MGMG}. These observations already give us a clue for the inter- and intrachain origin of the different peaks in the correlation functions.

Real Space Analysis: Inter- and Intrachain Contributions. Additional valuable information can be extracted from the radial distribution functions in real space. There we have distinguished inter- and intrachain contributions. The interchain contributions have been obtained by considering correlations among atoms of different chains, while the intrachain contributions arise from atoms belonging to the same chain. Figure 9 shows the results obtained at 300 K for selected representative atoms in the system: the main-chain carbons (C_{MC}) and the methyl group carbons (C_{MG}).

Starting with the main-chain carbons (Figure 9a), we can see that the intrachain contributions display a sequence of well-defined peaks only at quite short distances. The first (I) and second (II) peaks relate to the covalently bonded first and second carbon neighbors. The peaks related to the third neighbor are also very well developed. The one centered at $r = 3.2$ Å (III) reflects the position of the third neighbor in trans−gauche (t,g) conformation while the next peak (IV) at $r = 3.9$ Å arises from the corresponding all-trans state (t,t). From the peak areas the probabilities for the two conformations may be evaluated. They are 32% for trans and 68% for gauche. This means that the three isomeric conformations are almost equally probable. This explains the fast smearing of the further peaks. However, we can still assign the origin of the next peaks to certain conformations along

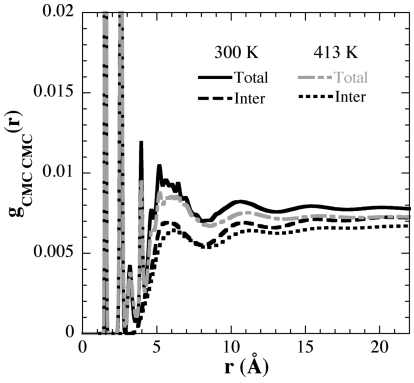

Figure 10. Total radial pair correlation function and its interchain contribution relating carbons in the main chain at the two extreme temperatures investigated.

the chain: peak V at 4.6 Å arises either from fourth neighbors separated by two consecutive trans followed by a gauche conformation or from fifth neighbors separated by (tg+tg+), (tg−tg−), (ttg+g+), or (tg+g+t) conformations. The sixth peak corresponds to fourth neighbors in all-trans conformation (ttt). Peaks VII, VIII, and IX arise from other fifth neighbors correlations: (tg+tt), (tg−tt), (tttg−), and (tttg+) to peak VII at 5.6 Å, (ttg+t) to peak VIII at 6 Å, and all-trans to peak IX at 6.45 Å. This analysis shows that PEP is a highly flexible polymer, in agreement with the values of C_∞ reported for this polymer in the literature (C_∞ is about 7 in the T range here explored).[48,49]

Turning to the interchain contribution of the correlation function $g_{C_{MC}C_{MC}}(r)$, it begins to show significant values only above 4 Å and displays a relatively broad peak at about 5.6 Å, which is characteristic for an amorphous structure with a distribution of interchain distances. The peak position roughly corresponds to the average interchain distance (5.1 Å) as estimated from the main peak of the MC/MC correlations in the Q-space (see Figure 8) by means of the Bragg approximation. We can also see a second—even broader—peak of this interchain contribution centered at about 11 Å. This peak would correspond to second-neighboring chains. In fact, inspecting further distances as shown in Figure 10, a third smooth and extremely broad peak can be envisaged; its maximum is located at about 16 Å, where a third chain would most probably be found. Thus, the value of about 5 Å obtained from the Bragg approximation for the average interchain distance corresponds well to the observed period in the modulation of the density due to interchain correlations. Moreover, we can see in Figure 9a that at distances of about 5 Å the predominant character of the contributing correlations to $g_{C_{MC}C_{MC}}(r)$ is of interchain origin. These observations support assigning a predominantly interchain origin to the first peak of A_{MCMC}. On the other hand, we note that the second peak in A_{MCMC} (see Figure 8, $Q_{2max}^{MCMC} = 2.95$ Å^{-1}, equivalent distance 2.13 Å) has to be related with the undulations of the intrachain correlation function, which show a much shorter period in space than those of the interchain correlations.

Temperature variations do not induce qualitative changes in $g_{C_{MC}C_{MC}}(r)$ (Figure 10). An increase in temperature influences the interchain part as shown in this figure: (i) it becomes smoother; the third peak is hardly seen—the system becomes more homogeneous—and (ii) the most probable first- and second-neighbor chain positions are shifted to larger distances. In the reciprocal space, this is reflected in the shift of the first peak of A_{MCMC} toward lower Q values. The intrachain correlations show a small decrease for distances longer

than ≈3.5 Å, indicating a further randomization of the conformations with increasing temperature.

Now we consider the methyl group carbons (Figure 9b). The interchain contribution to $g_{C_{MG}C_{MG}}(r)$ begins showing significant values at shorter distances than the interchain correlations of $g_{C_{MC}C_{MC}}(r)$. This reflects the fact that methyl groups of different chains can approach each other closer than main-chain atoms. In fact, the first correlation distance of about 4.2 Å coincides with the van der Waals distance between methane.[68] In the region of the first broad intermolecular peak of the main-chain carbons (distances below ≈8 Å) we can see in fact a second peak in the interchain part of $g_{C_{MG}C_{MG}}(r)$ (at around 6 Å), presumably due to MGMG pairs belonging to nearest-neighbor chains, but more separated than the main chains. An important observation is the clear periodicity of the interchain contribution to $g_{C_{MG}C_{MG}}(r)$ at larger distances. The mean separation between the third, fourth, and fith peaks is 4.75 Å. This would rise to a peak at $Q = 1.32$ Å^{-1}. We note that this is very close to the position of Q_{2max}^{MGMG}. This analysis strongly supports the hypothesis of an intermolecular origin for this peak, as suggested from the temperature dependence of the correlations in Q-space.

The intramolecular contributions to $g_{C_{MG}C_{MG}}(r)$ show a first small peak at 4 Å—at the same position as the intermolecular correlations. We note that this distance is too short to correspond to methyl groups belonging to consecutive monomers. Therefore, it has to be attributed to methyl groups on the same chain but not consecutive, after chain back-folding. The peaks between 5 and 8 Å can be assigned to consecutive methyl groups along the chain, though also some second methyl neighbors contribute in this region. In particular, the sharper peak at 6.9 Å can be attributed to first syndiotactic neighboring methyl groups separated by (ttt) conformations. At longer distances, the big variety of conformations and the atactic character of the chains lead to rather broad peaks with broad underlying distributions of distances.

Dynamics. Letting the system evolve with time, the short-range order is gradually lost. Computing the van Hove correlation function (eq 1) simulations allow observing directly in real space how the pair correlation functions smear out. Figure 11 shows the results for the main-chain carbons at 300 K. The total function tends to reach a constant value (determined by the average density) at long times. Only for the longest time considered in the figure, 50 ns, an almost flat function is observed. At 10 ns oscillations are still visible. This indicates that the structural relaxation time is in the range between these two times. This agrees with the value of 12 ns obtained for the characteristic time of the dynamic structure factor at the first structure factor peak (see Figure 7c). Splitting the van Hove correlation function in its inter- and intracontributions, we observe that the smearing of the long-distance correlations is mainly due to the decay of the interchain correlations (Figure 11c). On the contrary, the homogenization of the local structure (below ≈ 4 Å) is mainly governed by the intrachain contribution (Figure 11b). It is also worthy of remark how fast the well-defined intrachain peaks loose their sharpness, as can be appreciated in the inset of this figure. At 0.5 ps the peaks arising from third and further neighbors cannot be resolved anymore. In this time range, the only dynamic process taking place is the fast dynamics of the atoms prior to feeling the cage imposed by the neighbors.

Though the visualization of the van Hove correlation functions is very instructive, in the following we further discuss the dynamical aspects in terms of the intermediate scattering functions in the reciprocal space, which are—at least some of them, and, in particular, the dynamic structure factor—experimentally accessible. We will further exploit MD simulations to unravel the different contributions to the dynamic structure factor and look for the comparison between collective and self-correlation functions. Finally, we compare PEP behavior with reported results on other polymers and briefly discuss the support provided by this study to the mode coupling theory (MCT).[1]

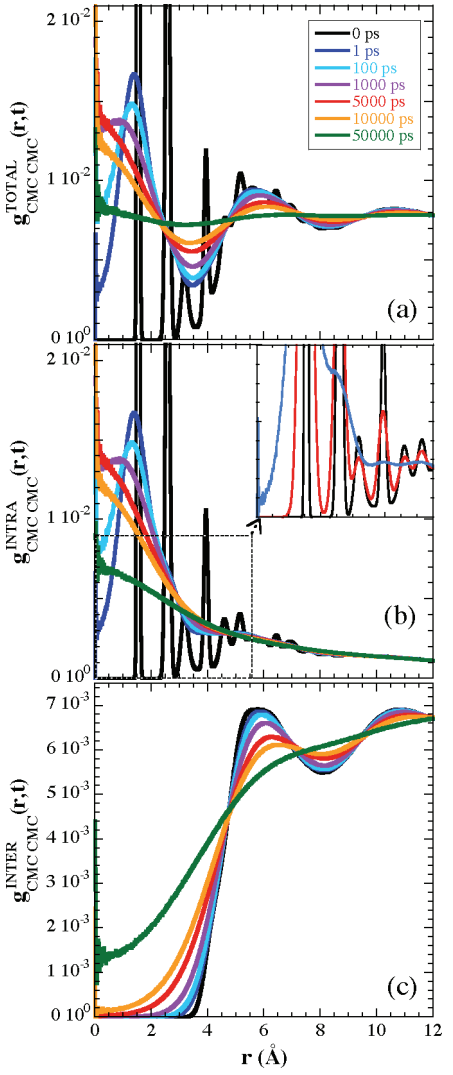

Figure 11. Time evolution of the pair correlation function of the main-chain carbons at 300 K for (a) the total function, (b) the intrachain, and (c) the interchain contributions. The inset in (b) is a zoom of the selected area where the function is represented at 0 (black), 0.1 (red), and 0.5 ps (blue).

Contributions to $S(Q,t)$. The previous analysis of the structure factor has proven that at its first peak the contributions from lateral groups are almost negligible compared with those arising from main-chain/main-chain correlations; moreover, the latter are mostly of interchain origin. Therefore, PEP is an ideal system to properly scrutinize the structural relaxation, and with our NSE measurements at Q_{1max} we should have indeed followed the genuine α-relaxation in an isolated way. MD simulations allow checking this statement.

For the intermediate temperature investigated, Figure 12a shows the normalized dynamic structure factor $S(Q,t)/S(Q)$ at the first structure factor peak and its contributions $A_{\alpha\beta}(Q,t)/S(Q)$ arising from the MCMC, MGMG, and cross-correlations.

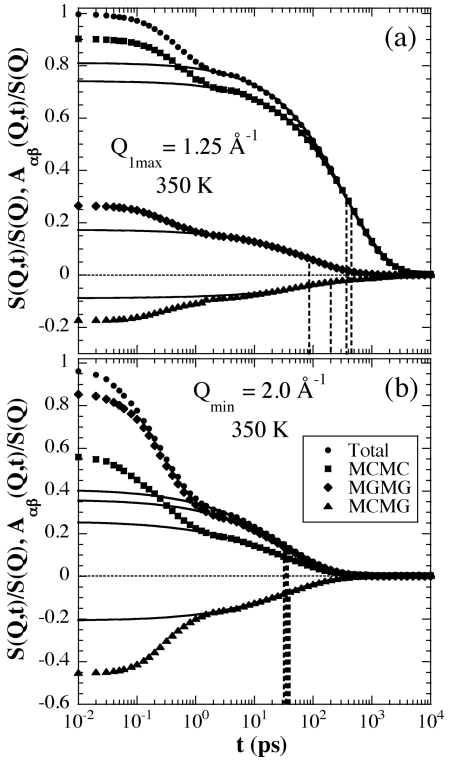

Figure 12. Dynamic structure factor $S(Q,t)$ and its contributions $A_{\alpha\beta}(Q,t)$, $\alpha\beta$ = MCMC, MGMG, and MCMG, normalized to the total static structure factor $S(Q)$ at 350 K calculated from MD simulations: (a) Q = 1.25 Å^{-1} ($\approx Q_{1max}$) and (b) Q = 2 Å^{-1}. Solid lines are fits to KWW functions. The horizontal dotted line marks the 0 value, and the vertical lines mark the positions of the KWW times.

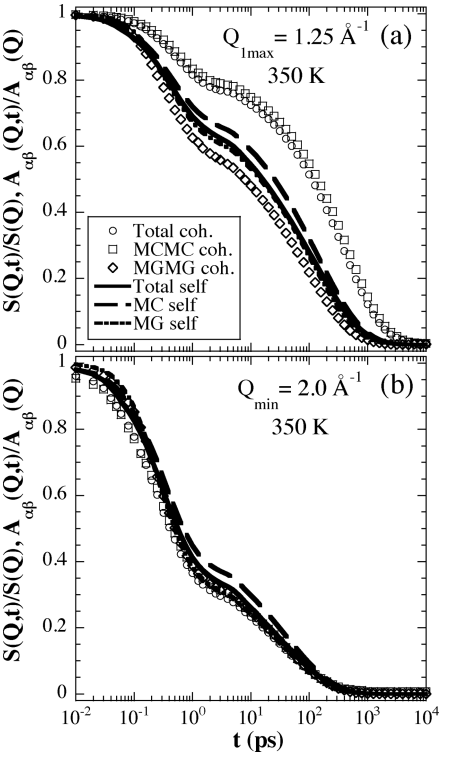

Figure 13. Dynamic structure factor and its contributions MCMC, MGMG, and MCMG (symbols) and their self-counterparts (lines) at 350 K calculated from MD simulations: (a) Q = 1.25 Å^{-1} ($\approx Q_{1max}$) and (b) Q = 2 Å^{-1} (close to the minimum). For the MG self-correlations only the carbon atoms were considered in order to avoid the contribution of the methy group rotations. All functions are normalized to their corresponding static values.

The static values of these contributions are those shown in Figure 8 normalized to the total structure factor. KWW fits of the slow decays of these functions show that the characteristic time scales of the three contributions are rather different: the MCMC correlations decay more than 4 times more slowly than the MGMG correlations. The cross-term shows an intermediate time scale. However, as the MCMC contribution overwhelmingly dominates, the dynamic structure factor reveals a time scale almost indistinguishable from that relating MC atoms of different chains.

Moving to higher Q values, Figure 12b shows that e.g. at Q = 2 Å^{-1} the situation is different. There, the three partial correlation functions decay nearly at the same time. Therefore, though the dominating term is that reflecting MGMG correlations, the time scale observed for the dynamic structure factor also coincides with that of the MCMC correlation function. As we will see below, this situation persists toward even higher Q values. The three correlation functions decay in a very similar way, also e.g. at the second structure factor maximum.

We have separately analyzed the partial correlation functions and their self-counterparts at 350 K. To avoid the contribution of methyl group rotations (which characteristic time scale is about 15 ps at 350 K[39]), for the MG self-correlations we have considered that of the carbon atom. Figure 13 shows these functions normalized to their static value, together with the total coherent and self-correlation functions for two Q values. At Q_{1max} we observe that (i) the amplitude and time scale of the slow decay of the collective MCMC correlation function are significantly larger than those of the self MC function, (ii) this is mirrored by the total functions, (iii) the collective and self-correlation functions involving MG atoms are rather similar, and (iv) the amplitudes and time scales of functions relating with MC are much larger than those obtained for the MG functions. At the higher Q value shown in Figure 13b we see very close results for all functions.

A characterization of the slow decays of these normalized functions in terms of KWW functions gives the values for the shape parameters, amplitudes, and time scales displayed in Figure 14.[69] We can deduce that (i) in general, coherency effects are most evident for MCMC correlations in the neighborhood of the first structure factor peak; (ii) within the scatter, the stretching parameter of the partial collective functions seems to mirror the corresponding static behavior; (iii) the β-parameter for the total self-correlation function is smaller than those of the MC and MG self-motions, reflecting the distribution of mobilities due to dynamic heterogeneity at atomic level; (iv) above $Q \approx 1.5$ Å^{-1} the results for the time scales are very close for all collective functions (and similar to that for the times of total and self-correlations); and (v) the decrease of the DWF and the β exponent of the total dynamic structure factor at low Q values is due to the interplay between different correlation functions, in particular to the negative sign and relatively large absolute value of the cross-correlation term. We finally note that in the high Q range, while coherency effects are lost in the slow decay, they are still appreciable in the DWF; i.e., at such short length scales coherency is still important in the fast-dynamics regime.

Relating Self and Collective functions. In the case of simple monatomic liquids, the coherent scattering function can easily be built starting from the self-counterpart. There, the

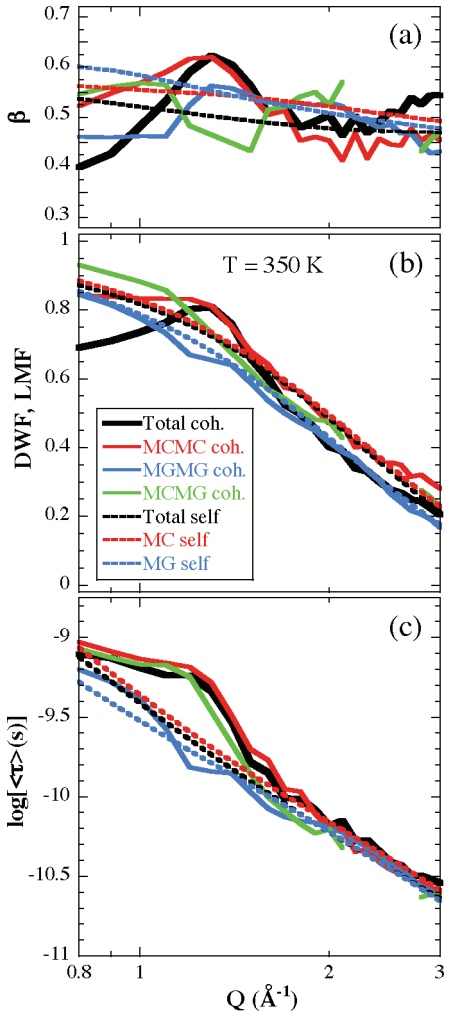

Figure 14. Momentum transfer dependence of the KWW parameters characterizing the slow decay of the simulated dynamic structure factor and its contributions, normalized to their corresponding static values (solid lines) at 350 K: (a) shape parameters, (b) amplitudes, and (c) average characteristic times. Dotted lines correspond to the same parameters for the normalized self-contributions.

coherent characteristic time shows the so-called deGennes narrowing[70]

$$\tau_{coh}(Q) = S(Q)\tau_{self}(Q) \qquad (9)$$

Here, $S(Q)$ has to be normalized to 1 for $Q \rightarrow \infty$. Figure 15a checks this prediction with the time scales of PEP obtained from the simulations. Though in the neighborhood of the first structure factor peak it reproduces rather well the slowing down of the collective with respect to the self-motions, it qualitatively fails above $Q \approx 1.5$ Å^{-1}. There, $S(Q)$ shows a minimum that would give rise to an acceleration of the collective dynamics with respect to self-motions, but the time scales are in fact almost indistinguishable. Below the peak it also predicts too faster collective time scales. A similar degree of agreement is shown in the case of the characteristic times for MCMC correlations when related through eq 9 with the corresponding self-time scales (Figure 15b). In this case, the role of $S(Q)$ is played by the corresponding normalized $A_{\alpha\beta}(Q)$ functions. However, for MGMG correlations the deGennes approach clearly fails in all the Q range investigated (Figure 15c).

We note that, according to the discussion on the temperature dependence of the structure factor and its components,

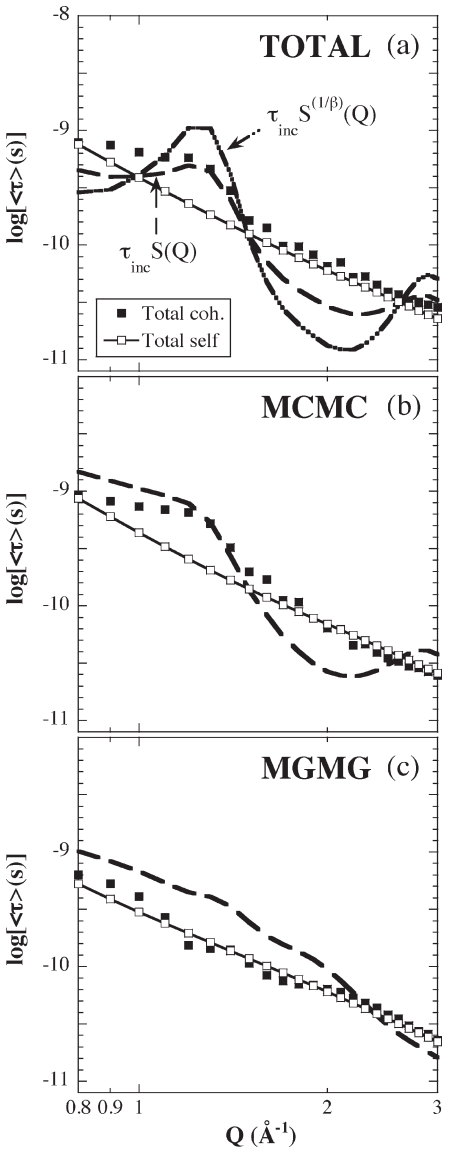

Figure 15. Check of the deGennes narrowing prediction (eq 9) (dashed lines) with the 350 K simulation results of Figure 14: (a) total, (b) MCMC, and (c) MGMG contributions. The full symbols are the coherent average characteristic times, and the empty symbols connected by lines are the incoherent ones from the self-parts. In (a) the generalized prediction (eq 10) is also represented (dashed-dotted line).

the correlations at Q above ≈1.5 Å^{-1} are mainly of intramolecular origin. Therefore, in such region an approach like that of deGennes is not expected to apply anymore.

We have tried to apply another approach suggested for stretched functional forms[71]

$$\tau_{coh}(Q) = S(Q)^{1/\beta}\tau_{inc}(Q) \qquad (10)$$

based on a Sköld-like ansatz.[72] As can be seen in Figure 15a, it provides an even worse description than that of deGennes, since it produces a sharper modulation with $S(Q)$ than that expected in the case of simple liquids.

Since the incoherent cross section of carbon is zero, it is impossible to access experimentally the self-part of the dynamic structure factor. The closest function measurable is the incoherent scattering function of hydrogens in a protonated sample. This was investigated in a previous work.[39] The experimental data were analyzed considering the simultaneous occurrence of vibrations, methyl group

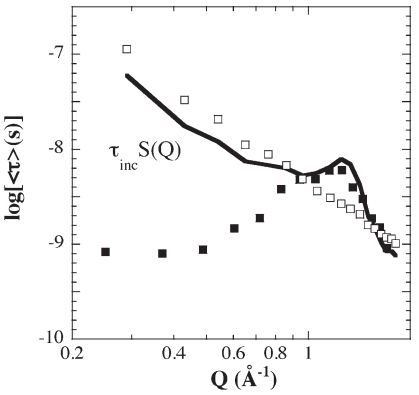

Figure 16. Check of the deGennes narrowing prediction (eq 9) (line) with experimental results at 300 K. The full symbols correspond to the coherent average characteristic times determined from the analysis of the collective motions (IN11 results), and the empty symbols are the average times for self-hydrogen motions involved in the α-relaxation (results from a protonated sample in a previous work[39]). The structure factor measured by D7 was used.

rotations, and segmental relaxation. This last was parametrized in terms of KWW functions with $\beta = 0.5$. In Figure 16 we have compared the so deduced average times for self-motions involved in the α-relaxation with those obtained in this work for collective motions. The temperature is 300 K. Using the experimentally determined structure factor, we have built the deGennes prediction (eq 9) shown as the line. We observe again a nice agreement in the neighborhood of the first structure factor peak, but severe deviations occur in the intermediate length scales regime. Obviously, new theoretical approaches are needed to reproduce and explain the behavior of the dynamic structure factor of polymers in this Q regime.

The deGennes narrowing was also checked in ref 73, where the dynamic structure factor of several polyolefins including PEP was investigated through united-atom simulations. The collective characteristic times of the slow decay showed a modulation with $S(Q)$ that was also overestimated by the simple approach of deGennes. In that work, the shape parameter was found to show a very week reminiscence of the structure factor, in apparent contradiction with our results. We note that those simulations were carried out at 423 K, a higher temperature than the highest here investigated. In such regime, the β values are difficult to estimate, specially at high Q.[67] In fact, from our results, the $S(Q)$ modulation seems to smear out at high temperatures, mainly in the high Q range. This would be well compatible with the behavior observed by Neelakantan and Maranas. Below the first structure factor peak, however, our results would indicate larger stretching than the united-atom model.

Comparison with Other Polymers. The combination of NSE and MD simulations to unravel the contributions to the dynamic structure factor has recently been applied to other two systems of more complex microstructure: PMMA[24] and PVAc.[25] In both cases, the first structure factor peak was identified to be of predominantly interchain character; however, it was quite difficult to relate the observed overall relaxation at that peak to the different partial structure functions. This is due to the rather strong contributions of several correlation functions involving side groups in the peak region. In particular, cross-correlations between main-chain atoms and atoms in lateral groups are as strong as the MCMC correlations, but with opposite sign. Thus, PEP provides a unique opportunity to practically isolate MCMC dynamics at the first structure factor peak.

For PMMA a much slower dynamics is observed for MCMC correlations than for the other correlators including its self-counterpart. This difference is most evident at the first peak (where deGennes narrowing does not reproduce the relationship between collective and self-correlations) but persists at higher Q values (close to the second peak at 1.9 $Å^{-1}$). The data were interpreted on the grounds that the side groups loose their correlation by rotational motion around the main-chain axis, while the main chains stay correlated. For the side groups the coherency effects observed at the first peak are lost at the second peak. In the case of PVAc, practically identical time scales are found for all collective functions, suggesting a more correlated dynamics between side groups and main chains also at intermolecular distances. The deGennes narrowing does not describe the coherency effects observed at the first maximum, which are absent in the neighborhood of the second peak (mostly intramolecular in nature). PEP shows an intermediate behavior. MCMC correlations at the intermolecular peak display a slower dynamics than the MGMG correlations (factor of about 4 for PEP against the 10 times observed for PMMA). On the other hand, the deGennes relation does hold for PEP in the close neighborhood of Q_{1max}—contrary to the other polymers. As for PVAc, coherency effects seem to disappear as soon as the correlations become of intramolecular nature.

Finally, we mention the experimental results here obtained in the intermediate length-scales region. Because of the low intensities of the signal involved, this region of the dynamic structure factor is almost unexplored. The only reported data until now are those corresponding to PIB.[17] In that polymer, a similar $S(Q)$ modulation of the apparent activation energy of the characteristic relaxation time of the slow decay was also reported. Whether this is a general feature of polymer dynamics is an important open question deserving future experimental studies.

Mode Coupling Theory. A thorough check of MCT predictions is beyond the scope of this work. However, we can state that the results here obtained show a nice agreement with some general predictions of the MCT. In particular, we underline the favorable condition offered by PEP to isolate the intermolecular main-chain/main-chain correlations at the first structure factor peak, which is not trivial in other more complex polymers. In this way, NSE provides the experimental way to univocally follow the structural relaxation. The predicted viscosity scaling and stretching of the dynamic structure factor are obviously perfectly fulfilled by the α-relaxation in PEP (see Figure 4a). The temperature-independent value of the DWF (nonergodicity parameter in the MCT terminology) would support the MCT prediction above the critical temperature T_c. This temperature should be located around $1.2T_g = 255$ K.

We also note that the $S(Q)$ modulation of the nonergodicity factor and the time scale of the slow process is in qualitative agreement with the MCT scenario. The reflection of the first structure factor peak in these parameters would underline the cooperative nature of the glass transition.

Conclusions

By the combination of neutron scattering and MD simulations, we have investigated the short-range order and the dynamic structure factor of PEP in a wide Q range including the intermediate length scales region, the first and the second static structure factor peaks spanning thus over inter- and intramolecular length scales. Our most salient results are the following:

- We have thoroughly disentangled the short-range order in this polymer. Of utmost help have been the

direct insight in real-space and the separation of inter- and intrachain contributions facilitated by the MD simulations.

- The first peak of $S(Q)$ is clearly dominated by MCMC contributions (MGMG and cross-correlation terms are very weak there). At this peak, the correlations are of interchain origin. Therefore, $S(Q_{1max},t)$ reveals directly the dynamics leading to the decay of the correlations between atoms of different chain backbones—the genuine α-relaxation. We note that this is not necessarily true in other polymers.[24,25]
- The direct observation of the α-relaxation in this way has allowed establishing the viscosity scaling, the stretching, the time−temperature superposition, and the deGennes narrowing.
- An in-phase modulation with $S(Q)$ is observed for the amplitude and the shape parameter of the slow decay of the dynamic structure factor around the first peak. The time scales also present a maximum in this region that with varying temperature shifts in a much more dramatic way than the structure factor. Interestingly, the apparent activation energy of the characteristic time mirrors the Q dependence of $S(Q)$. Thus, in the intermediate length scales region we find a significantly weaker temperature dependence than that of the viscosity.
- Coherency effects are lost in the Q region where intramolecular correlations dominate (above $\approx$1.5 $Å^{-1}$). There, deGennes narrowing naturally fails.

Acknowledgment. We thank the Institut Laue-Langevin (ILL) for neutron facilities as well as Drs. P. Fouquet, M. Maccarini, and A. P. Murani at the ILL and Dr. W. Schweika in Jülich for experimental support. The European Commission, NMI3 Contract RII3-CT-2003-505925, supported the experiments at the Forschungsreaktor in Jülich. We thank support by the "Donostia International Physics Center", the European Commission NoE SoftComp, Contract NMP3-CT-2004-502235, the projects MAT2007-63681 and IT-436-07 (GV), and the Spanish Ministerio de Educacion y Ciencia (Grant CSD2006-53). R.P.-A. acknowledges Grant BES-2005-10794 (MAT2004-01017).

References and Notes

(1) Götze, W. In *Liquids, Freezing, Glass Transition*; Hansen, J. P., Levesque, D., Zinn-Justin, J., Eds.; North-Holland: Amsterdam, 1991; p 287.
(2) Götze, W.; Sjögren, L. *Rep. Prog. Phys.* **1992**, *55*, 241.
(3) Götze, W. *J. Phys.: Condens. Matter* **1999**, *11*, A1.
(4) Mezei, F.; Knaak, W.; Farago, B. *Phys. Rev. Lett.* **1987**, *58*, 571.
(5) Bartsch, E.; Fujara, F.; Legrand, J. F.; Petry, W.; Sillescu, H.; Wuttke, J. *Phys. Rev. E* **1995**, *52*, 738.
(6) Tölle, A.; Schober, H.; Wuttke, J.; Fujara, F. *Phys. Rev. E* **1997**, *56*, 809.
(7) Tölle, A.; Wuttke, J.; Schober, H.; Randall, O. G.; Fujara, F. *Eur. Phys. J. B* **1998**, *5*, 231.
(8) Wuttke, J.; Petry, W.; Coddens, G.; Fujara, F. *Phys. Rev. E* **1995**, *52*, 4026.
(9) Wuttke, J.; Petry, W.; Pouget, S. *J. Chem. Phys.* **1996**, *105*, 5177.
(10) Richter, D.; Frick, B.; Farago, B. *Phys. Rev. Lett.* **1988**, *61*, 2465.
(11) Buchenau, U.; Monkenbusch, M.; Stamm, M.; Majkrzak, C. F.; Nücker, N. In *Polymer Motion in Dense Systems*; Richter, D., Springer, T. Eds.; Proceedings in Physics Vol. *29*; Springer: Berlin, 1988; p 138.
(12) Arbe, A.; Colmenero, J. *Phys. Rev. E*, in press.
(13) Holzer, B.; Strobl, G.; Stühn, B.; Andersen, N. H. *Colloid Polym. Sci.* **1994**, *272*, 1396.
(14) Arbe, A.; Buchenau, U.; Willner, L.; Richter, D.; Farago, B.; Colmenero, J. *Phys. Rev. Lett.* **1996**, *76*, 1872.
(15) Arbe, A.; Richter, D.; Colmenero, J.; Farago, B. *Phys. Rev. E* **1996**, *54*, 3853.
(16) Zorn, R.; Richter, D.; Farago, B.; Frick, B.; Kremer, F.; Kirst, U.; Fetters, L. J. *Physica B* **1992**, *180−181*, 534.
(17) Farago, B.; Arbe, A.; Colmenero, J.; Faust, R.; Buchenau, U.; Richter, D. *Phys. Rev. E* **2002**, *65*, 051803.
(18) Richter, D.; Arbe, A.; Colmenero, J.; Monkenbusch, M.; Farago, B.; Faust, R. *Macromolecules* **1998**, *31*, 1133.
(19) Arrighi, V.; Pappas, C.; Triolo, A.; Pouget, S. *Physica B* **2001**, *301*, 157.
(20) Faivre, A.; Levelut, C.; Durand, D.; Longeville, S.; Ehlers, G. *J. Non-Cryst. Solids* **2002**, *307−310*, 712.
(21) Arbe, A.; Moral, A.; Alegría, A.; Colmenero, J.; Pyckhout-Hintzen, W.; Richter, D.; Farago, B.; Frick, B. *J. Chem. Phys.* **2002**, *117*, 1336.
(22) Richter, D.; Monkenbusch, M.; Arbe, A.; Colmenero, J. *Neutron Spin Echo in Polymer Systems*; Adv. Polym. Sci. Vol. *174*; Springer-Verlag: Berlin, 2005.
(23) Richter, D.; Monkenbusch, M.; Willner, L.; Arbe, A.; Colmenero, J.; Farago, B. *Europhys. Lett.* **2004**, *66*, 239.
(24) Genix, A. C.; Arbe, A.; Alvarez, F.; Colmenero, J.; Farago, B.; Wischnewski, A.; Richter, D. *Macromolecules* **2006**, *39*, 6260.
(25) Tyagi, T.; Arbe, A.; Alvarez, F.; Colmenero, J.; González, M. A. *J. Chem. Phys.* **2008**, *129*, 224903.
(26) Brodeck, M.; Alvarez, F.; Arbe, A.; Juranyi, F.; Unruh, T.; Holderer, O.; Colmenero, J.; Richter, D. *J. Chem. Phys.* **2009**, *130*, 094908.
(27) Furuya, H.; Mondello, M.; Yang, H.-J.; Roe, R.-J.; Erwin, R. W.; Han, C. C.; Smith, S. D. *Macromolecules* **1994**, *27*, 5674.
(28) Ward, D. J.; Mitchell, G. R. *Phys. Scr.* **1995**, *T57*, 153.
(29) Eilhard, J.; Zirkel, A.; Tschöp, W.; Hahn, O.; Kremer, K.; Schärpf, O.; Richter, D.; Buchenau, U. *J. Chem. Phys.* **1999**, *110*, 1819.
(30) Alvarez, A.; Colmenero, J.; Zorn, R.; Willner, L.; Richter, D. *Macromolecules* **2003**, *36*, 238.
(31) Narros, A.; Arbe, A.; Alvarez, F.; Colmenero, J.; Zorn, R.; Schweika, W.; Richter, D. *Macromolecules* **2005**, *38*, 9847.
(32) Genix, A. C.; Arbe, A.; Alvarez, F.; Colmenero, J.; Schweika, W.; Richter, D. *Macromolecules* **2006**, *39*, 3947.
(33) Iradi, I.; Alvarez, F.; Colmenero, J.; Arbe, A. *Physica B* **2004**, *350*, E881.
(34) Moe, N. E.; Ediger, M. D. *Phys. Rev. E* **1999**, *59*, 623.
(35) Colmenero, J.; Alvarez, F.; Arbe, A. *Phys. Rev. E* **2002**, *65*, 041804.
(36) Colmenero, J.; Alvarez, F.; Arbe, A.; Narros, A.; Monkenbusch, M.; Richter, D. *Europhys. Lett.* **2005**, *71*, 26.
(37) Colmenero, J.; Narros, A.; Alvarez, F.; Arbe, A.; Moreno, A. J. *J. Phys.: Condens. Matter* **2007**, *19*, 205127.
(38) Narros, A.; Arbe, A.; Alvarez, F.; Colmenero, J.; Richter, D. *J. Chem. Phys.* **2008**, *128*, 224905.
(39) Pérez-Aparicio, R.; Arbe, A.; Colmenero, J.; Frick, B.; Willner, L.; Richter, D.; Fetters, L. J. *Macromolecules* **2006**, *39*, 1060.
(40) Sun, H.; Rigby, D. *Spectrochim. Acta* **1997**, *A153*, 1301.
(41) Rigby, D.; Sun, H.; Eichinger, B. E. *Polym. Int.* **1997**, *44*, 311.
(42) Sun, H. *J. Phys. Chem. B* **1998**, *102*, 7338.
(43) Sun, H.; Ren, P.; Fried, J. R. *Comput. Theor. Polym. Sci.* **1998**, *8*, 229.
(44) Bunte, S. W.; Sun, H. *J. Phys. Chem. B* **2000**, *104*, 2477.
(45) Yang, J.; Ren, Y.; Tian, A.; Sun, H. *J. Phys. Chem. B* **2000**, *104*, 4951.
(46) McQuaid, M. J.; Sun, H.; Rigby, D. *J. Comput. Chem.* **2004**, *25*, 61.
(47) Theodorou, D. N.; Suter, U. W. *Macromolecules* **1985**, *18*, 1467.
(48) Fetters, L. J.; Lohse, D. J.; Richter, D.; Witten, T. A.; Zirkel, A. *Macromolecules* **1994**, *27*, 4639.
(49) Fetters, L. J.; Lohse, D. J.; Colby, R. H. In *Physical Properties of Polymers Handbook*, 2nd ed.; Mark, J. E., Ed.; Springer: New York, 2007; Chapter 25.
(50) Morton, M.; Fetters, L. J. *Rubber Chem. Technol.* **1975**, *48*, 359.
(51) Hadjichristidis, N.; Iatrou, H.; Pispas, S.; Pitsikalis, M. *J. Polym. Sci., Part A: Polym. Chem.* **2000**, *38*, 3211.
(52) Stewart, J. R.; Deen, P. P.; Andersen, K. H.; Schober, H.; Barthelemy, J. F.; Hillier, J. M.; Murani, A. P.; Hayes, T.; Lindenau, B. *J. Appl. Crystallogr.* **2009**, *42*, 69.
(53) Mezei, F. *Neutron Sin Echo, Lecture Notes in Physics*; Springer-Verlag: Heidelberg, 1980; Vol. *28*.
(54) Frick, F.; Richter, D.; Ritter, Cl. *Europhys. Lett.* **1989**, *9*, 557.
(55) Misawa, M.; Kanaya, T.; Fukunaga, T. *J. Chem. Phys.* **1991**, *94*, 8413.
(56) Londono, J. D.; Annis, B. K.; Habenschuss, A.; Smith, G. D.; Borodin, O.; Tso, C.; Hsieh, E. T.; Soper, A. K. *J. Chem. Phys.* **1999**, *110*, 8786.

(57) Johnson, J. A.; Saboungi, M. L.; Price, D. L.; Ansell, S.; Russell, T. P.; Halley, J. W.; Nielsen, B. *J. Chem. Phys.* **1998**, *109*, 7005.
(58) Frick, B.; Alba-Simionesco, C.; Andersen, K. H.; Willner, L. *Phys. Rev. E* **2003**, *67*, 051801.
(59) Mondello, M.; Yang, H.-J.; Furuya, H.; Roe, R.-J. *Macromolecules* **1994**, *27*, 3566.
(60) Ayyagari, C.; Bedrov, D.; Smith, G. D. *Macromolecules* **2000**, *33*, 6194.
(61) Placzek, G. *Phys. Rev.* **1952**, *86*, 377.
(62) Yarnell, J. L.; Katz, M. J.; Wenzel, R. G.; Koenig, S. H. *Phys. Rev. A* **1974**, *7*, 2130.
(63) We have assumed the same inelasticity effects for the coherent and the incoherent contributions and independent of the deuteration level. We note that in any case they are very small (Figure 1a).
(64) Arbe, A.; Colmenero, J.; Alvarez, F.; Monkenbusch, M.; Richter, D.; Farago, B.; Frick, B. *Phys. Rev. E* **2003**, *67*, 051802.
(65) Narros, A.; Alvarez, F.; Arbe, A.; Colmenero, J.; Richter, D.; Farago, B. *J. Chem. Phys.* **2004**, *121*, 3282.
(66) Gell, C. B.; Graessley, W. W.; Fetters, L. J. *J. Polym. Sci., Part B: Polym. Phys.* **1997**, *35*, 1933.
(67) In the high-Q range ($Q > 1.5$ Å^{-1}) at the highest temperature investigated, the time scale of this decay is below 2 ps. Therefore, the fit of the dynamic structure factor is not reliable anymore because the values of the shape and the amplitude parameters are floating simultaneously. There, the values of the shape parameter have been fixed to those determined from the self-part of the function.
(68) Press, W. *J. Chem. Phys.* **1972**, *56*, 2597.
(69) Because of the low amplitude of the cross-term MCMG around 2.5 Å^{-1}, it was not possible to fit the data in this region.
(70) de Gennes, P. G. *Physica* **1959**, *25*, 825.
(71) Arbe, A.; Colmenero, J.; Richter, D. In *Broad Band Dielectric Spectroscopy*; Kremer, F., Schönhals, A., Eds.; Springer-Verlag: Heidelberg, 2002; p 685.
(72) Sköld, K. *Phys. Rev. Lett.* **1967**, *19*, 1023.
(73) Neelakantan, A.; Maranas, J. K. *J. Chem. Phys.* **2004**, *120*, 1617.